



Sustainable hydrogen peroxide production based on dopamine through Janus-like mechanism transition from chemical to photocatalytic reactions



Do-Yeon Lee ^{a,1}, Minju Park ^{b,1}, Namhee Kim ^b, Minsu Gu ^{c,*}, Hyoung-il Kim ^{a,*}, Byeong-Su Kim ^{b,*}

^aSchool of Civil and Environmental Engineering, Yonsei University, Seoul 03722, Republic of Korea

^bDepartment of Chemistry, Yonsei University, Seoul 03722, Republic of Korea

^cDepartment of Chemical Engineering (BK21 FOUR), Dong-A University, Busan 49315, Republic of Korea

ARTICLE INFO

Article history:

Received 31 March 2022

Revised 14 May 2022

Accepted 24 May 2022

Available online 28 May 2022

Keywords:

Dopamine

Polydopamine

Photocatalysts

Hydrogen peroxide

ABSTRACT

With increasing interest in hydrogen peroxide (H₂O₂) as an environmentally friendly oxidant for environmental remediation and a promising liquid fuel, we present herein a novel method for green and sustainable H₂O₂ production using versatile dopamine-based materials, demonstrating the conversion of H₂O₂ generation mechanism from a chemical to a photocatalytic process along with the structural transformation of dopamine to polydopamine. During the auto-oxidation of dopamine in the presence of oxygen, which involved the transition of catechol to hydroquinone groups and the ring closure of the amine group, H₂O₂ was chemically generated at a rate of 1.61 mmol g⁻¹h⁻¹ without an extra electron donor and additional energy sources. In contrast, self-polymerized polydopamine exhibited an effective photocatalytic H₂O₂ generation at a rate of 0.53 mmol g⁻¹h⁻¹ owing to its visible light absorptivity and semi-conducting property. We anticipate that these unique properties of dopamine will provide a new class of organic-based, highly efficient solar-to-H₂O₂ conversion and sustainable energy systems in the future.

© 2022 Elsevier Inc. All rights reserved.

1. Introduction

Hydrogen peroxide (H₂O₂) is a useful oxidant and carbon-free energy carrier that has been extensively utilized in many industrial and environmental processes [1–4]. Currently, the mass production of H₂O₂ is achieved via the anthraquinone process, involving expensive noble metal catalysts, hydrogen gas, and organic byproducts [5,6]. Given the limitations of existing H₂O₂ production technologies that are chemically demanding and not carbon neutral, an environmentally favorable and benign approach for the production of H₂O₂ is highly desirable.

On the contrary, the photocatalytic H₂O₂ production approach is appealing to overcome the aforementioned limitations because it only requires water, oxygen, and sunlight [7]. In this context, metal-free photocatalysts have emerged as a new class of catalysts for the production of H₂O₂ by virtue of their attractive chemical and photophysical properties, which differ from those of conventional metal-based photocatalysts [8–10]. However, despite this

recent progress, H₂O₂ production is still challenging due to a number of drawbacks, including a low active surface area, insufficient light harvesting, and, more importantly, rapid recombination of the photoinduced electron-hole pairs [11,12]. Therefore, several methods have been developed by controlling the chemical and structural properties of organic-based photocatalysts to overcome the limitations of solar-driven photocatalytic H₂O₂ generation [11]. For example, carbon nitride (C₃N₄)-based photocatalytic nanocomposites have been used because of their highly selective two-electron pathway in the oxygen reduction reaction (ORR) [11]. However, multiple synthetic processes to design the desired carbon nanomaterials at the nanoscale level can impose high economic costs compared to bio-inspired natural materials, which are more environmentally friendly and cost-effective. More recently, a few cases have used organic-based molecules or polymers as the aqueous photosubstrate or photoelectrocatalysts for producing H₂O₂ [13–18]. However, it still far from current necessary and sufficient condition since the photo-degradable substrates often suffer from critical issues such as separation process of product and recycling process of active materials. Moreover, there previous researches have required additional biased potential and electron donors to initiate the oxygen reduction reaction. In this context, it is essential to discover a novel organic-based candidate

* Corresponding authors.

E-mail addresses: sbgms@dau.ac.kr (M. Gu), hi.kim@yonsei.ac.kr (H.-i. Kim), bskim19@yonsei.ac.kr (B.-S. Kim).

¹ These authors contributed equally to this work.

and rational strategies toward environmentally benign and effective photocatalysts to produce H₂O₂.

As a key neurotransmitter and hormone *in vivo*, dopamine, with a catechol structure containing amine groups, has been intensively studied, especially in the field of surface chemistry owing to its mussel-inspired adhesive property [19]. Additionally, dopamine undergoes a self-polymerization process in a basic environment (pH greater than 8) with O₂ under ambient conditions to form polydopamine (PDA) [20]. Although the precise chemical structure of PDA is still elusive due to its various components, including catechol, amine, imine, and indole groups [21], PDA displays unique and versatile adhesion properties and thus has a high potential for biomedical applications. In addition to these adhesive properties, PDA exhibits semiconducting properties with broad absorption ranging from UV to visible light [22,23]. However, studies on the semiconducting properties of PDA have mainly focused on its applications as an additive component, such as a sensitizer or passivator in photocatalytic hybrids [24–26]. Besides, there are only few studies on H₂O₂ generation and exploring its underlying mechanisms based on catechol groups as active sites for oxygen reduction to H₂O₂, which ultimately takes place through the oxidation of dopamine and photocatalysis of PDA.

In this regard, herein we demonstrate a novel strategy for sustainable H₂O₂ production via the utilization of the unique ambivalent properties of dopamine: (1) chemical H₂O₂ production via the auto-oxidation of dopamine without any light irradiation and (2) visible-light-driven photocatalytic H₂O₂ production of PDA via photoactive reduction of O₂ (Scheme 1). Specifically, we investigated the efficient catalytic performance of H₂O₂ evolution even without electron donors—highly desired in conventional processes—and the formation mechanism involved in the structural transition of dopamine and PDA, which was achieved by the oxidation of catechol and the cyclization of amine. Because of its pH-dependent dispersibility and adhesion ability, PDA demonstrated the advantages of heterogeneous photocatalysts for recyclability and a versatile electrode coating regardless of any kinds of substrates. To date, a few studies have been reported toward photocatalytic H₂O₂ production with carbon based materials (Table S1). PDA exhibited high activity for photocatalytic H₂O₂ generation even without any electron donors, and it is comparable to metal-free semiconductors reported (Table S1). We anticipate naturally derived dopamine and PDA provides a new insight for a development of cost-effective and sustainable green photocatalysts to achieve high solar-to-H₂O₂ conversion platforms.

2. Experimental section

2.1. Materials

Dopamine hydrochloride, 3,4-dimethoxyphenyl ethylamine (PEA), 3,4-dihydroxyphenyl propanoic acid (PPA), indole, 5,6-dihydroxyindole (DHI), sulfuric acid, hydrochloric acid, perchloric acid, sodium phosphate monobasic dehydrate (98%), sodium phosphate dibasic dehydrate (98+%), ammonium solution, N,N-diethyl-1,4-phenylenediamine sulfate (DPD), horseradish peroxidase (POD, type VI-A), ethyl alcohol (EtOH), potassium hydroxide, and isatin were purchased from Sigma-Aldrich and used without further purification. Nickel (Ni) foam, glass substrate, titanium (Ti) foil, graphite foil, and polyethylene terephthalate (PET) sheet were purchased from Sj-material, Youth Tech Co., Sigma-Aldrich, Alfa Aesar, and Good-Fellow Co., respectively.

2.2. Synthesis of polydopamine (PDA)

PDA was synthesized through the oxidation and self-polymerization of dopamine in an alkaline water–ethanol aqueous

environment. Briefly, ethanol (40 mL) and deionized (DI) water (90 mL) were mixed with an aqueous ammonia solution (0.60 mL, 25–28%) for 30 min, and the pH was adjusted to approximately 11.3. Dopamine hydrochloride (0.50 g) was dissolved in DI water (10 mL). Subsequently, this dopamine solution was slowly added directly to the water–ethanol solvent. The color of the mixture gradually became dark brown. The reaction proceeded for 30 h. Furthermore, the product was centrifuged and washed with DI water and ethanol three times. The obtained product was freeze-dried for 24 h. Moreover, PDA was coated on various substrates (Ni foam, glass, Ti foil, graphite foil, and PET) under the same condition with PDA synthesis. Subsequently, the substrates were dipped in dopamine solution and then stirred for 30 h. After coating, the PDA-coated films were washed with DI water and dried at room temperature.

2.3. Characterizations

A UV/vis spectrophotometer (UV-2550, Shimadzu) was used to measure the absorbance and band gap evaluation. Ultraviolet photoelectron spectroscopy (UPS) (AXIS-NOVA, Kratos Inc.) was used to measure the energy levels. Moreover, the chemical structure was analyzed by XPS (K-alpha, Thermo Fisher). The morphology and size of the PDA were measured using SEM. The band gap (E_g) of material was calculated using the following equation where α is absorption coefficient, h is the Planck constant, ν is the photon's frequency, B is a constant, and E_g is the band gap energy. n is equal to 2 or 1/2 for the direct and indirect transition band gaps, respectively [27].

$$(\alpha h\nu)^n = B(h\nu - E_g)$$

2.4. Photocatalytic H₂O₂ Production

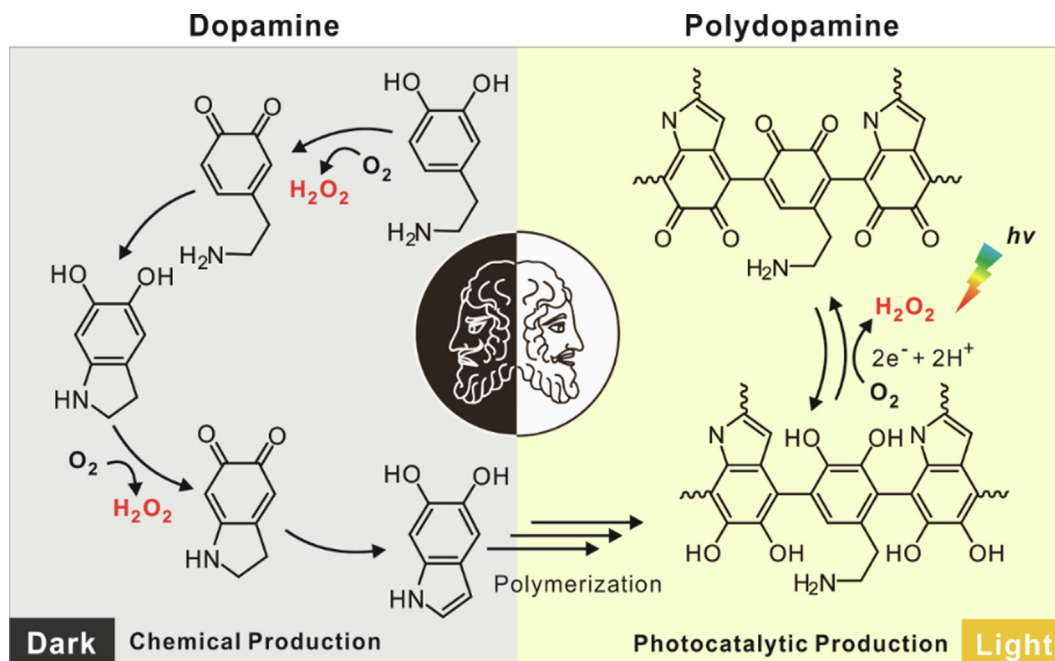
Photocatalytic H₂O₂ production experiments were performed by irradiating an aqueous suspension of various dopamine and PDA samples or PDA-coated substrates with simulated solar light (AM 1.5, 100 mW cm⁻²) from a 150-W xenon arc lamp in the presence or absence of 10 vol% ethanol as an electron donor. The incident light intensity was determined using a Newport calibrated Si solar cell. A sample aliquot was collected from the reaction suspension using a syringe. A DPD colorimetric method was also used to measure quantitative H₂O₂ production (at 551 nm, $\epsilon = 21000 \text{ M}^{-1} \text{ cm}^{-1}$, the detection limit in the range of 0.20–0.30 $\mu\text{g/L}$) [28]. Multiple experiments were independently conducted for all the photocatalytic tests. AQY was measured by irradiating the suspension of PDA in the presence of ethanol with monochromatic light ($\lambda = 280, 350, 420, 510, 570, \text{ and } 600 \text{ nm}$).

$$\text{AQY (\%)} = \frac{[\text{H}_2\text{O}_2 \text{ formed}] \times 2}{[\text{photon number entered into the reactor}]} \times 100$$

Theoretical maximum of H₂O₂ production rate (Fig. 1c) was determined as the equation presented below, assuming that 1 mol of dopamine generates 2 mol of H₂O₂ in process of self-oxidizing to DHI.

$$\begin{aligned} \text{Theoretical maximum H}_2\text{O}_2 \text{ production rate } (\mu\text{M}) \\ = [\text{Dopamine in reaction}](\mu\text{M}) \times 2 \end{aligned}$$

Electrochemical analysis was performed with a Pt wire and a Ag/AgCl electrode as the counter and reference electrodes, respectively. The working electrodes were used with FTO coated PDA, where 1 cm² of electrode was irradiated under 1-sun. Cyclic voltammetry (CV) was measured from –1.2 V to 0 V in PBS (0.1 M, pH 7) in 50 mV s⁻¹. Electrochemical impedance spec-



Scheme 1. Schematic Illustration of the Sustainable Production of H_2O_2 based on the Janus-like Pair of Dopamine and PDA; Chemical H_2O_2 Production by Dopamine under Dark and Photocatalytic H_2O_2 Production by PDA under Light Illumination.

troscopy (EIS) was measured at a bias of -0.8 V (vs. Ag/AgCl) in same electrolyte with CV. The range of frequency is 10 mHz to 100 kHz.

3. Results and discussion

3.1. Chemical H_2O_2 production of dopamine

To examine the H_2O_2 production performance of dopamine via an auto-oxidation reaction, we tested various reaction conditions, such as the presence of light and the electron donor (e.g., ethanol) (Fig. 1). The production rate and efficiency are generally enhanced under irradiation and in the presence of electron donor conditions in light-responsive materials. However, significant H_2O_2 production ($1.61 \text{ mmol g}^{-1} \text{ h}^{-1}$) was verified using dopamine without both light and electron donors. The presence of light and ethanol was notably detrimental to the H_2O_2 production over dopamine because of the loss of more than 50% of H_2O_2 ($0.62 \text{ mmol g}^{-1} \text{ h}^{-1}$) (Fig. 1a,b). These results imply that the mechanism of H_2O_2 production from dopamine involves a chemical reaction rather than a photocatalytic reaction, as reported in the literature regarding other dopamine-based materials where dopamine undergoes a self-oxidation reaction under an O_2 atmosphere [19]. In other words, the absorption of incident light by dopamine reduced the overall number of active sites for H_2O_2 production (i.e., catechol moieties of dopamine) by the photochemical transformation of catechol to quinone moieties via a radical reaction [9,29]. In the presence of ethanol, the production of H_2O_2 decreased to 75.4% under dark conditions, which could be attributed to the fact that alcohol acts as an inhibitor of the auto-oxidation process by preventing the transformation of dopamine to aminochrome—an essential intermediate of the auto-oxidation process—as observed for monoamine oxidase and catechol *ortho*-methyl transferase in vivo [19,30].

We investigated the UV/vis absorption spectra of dopamine over the course of the reaction in the absence of light irradiation and ethanol to clarify the structural transformation of dopamine during the auto-oxidation process (Fig. S1a). An increase in absor-

bance was noticeable at the wavelengths of 310 and 480 nm (Fig. S1c,d), wherein the peak at 310 nm corresponds to an $n-\pi^*$ electron transition associated with $\text{C}=\text{O}$ bonds in a typical aromatic ring [31]. In addition, the broad absorption at 480 nm is assigned to the formation of aminochrome [32], which is one of the oxidized forms of dopamine; the possible chemical structures formed during the dopamine auto-oxidation are depicted in Fig. 1d. It is widely known that the catechol group in dopamine is the active site for O_2 reduction [33]. Upon oxidation of dopamine, the one-electron oxygen reduction reaction (ORR) occurs; it involves dehydrogenation of the catechol group of dopamine, leading to the generation of superoxide anion radical and dopamine *o*-semiquinone radical [19]. With the subsequent oxidation of dopamine, the as-formed superoxide anion radical further transforms into H_2O_2 through an additional reduction reaction [19,34]. The oxidized catechol moieties (i.e., 1,2-benzoquinone) are recovered to yield the catalytically active catechol groups after cyclization of the amine group to afford the aminochrome structure, generating another H_2O_2 molecule through a second ORR process, followed by the formation of 5,6-dihydroxyindole (DHI) [33–36]. In addition, decomposition rate of H_2O_2 was not significantly observed in the case of dopamine and DHI (Fig. S2), making it clear that produced H_2O_2 was not affected during the oxidation process.

Based on this successive two-step H_2O_2 generation through the chemical oxidation of dopamine to yield DHI, we evaluated the long-term (24 h) production of H_2O_2 in the presence and absence of ethanol, with alternating O_2 and Ar saturation every 3 h under dark conditions (Fig. 1c). The results manifest that the dissolved O_2 was involved in the formation of H_2O_2 , indicating the occurrence of the chemical ORR mechanism. It was found that the amount of H_2O_2 produced gradually increased under the saturated O_2 conditions, reaching a saturation level of approximately $250 \mu\text{M}$ over 24 h. Interestingly, this value is close to the theoretically maximum H_2O_2 production calculated for an initial dopamine loading of 25.1 mg (corresponding to $264 \mu\text{M}$ of H_2O_2). In addition, the H_2O_2 production rate in the absence of ethanol was approximately twice as high as that observed in the presence of ethanol for 24 h. It can be explained by the inhibition of the cyclization of amine

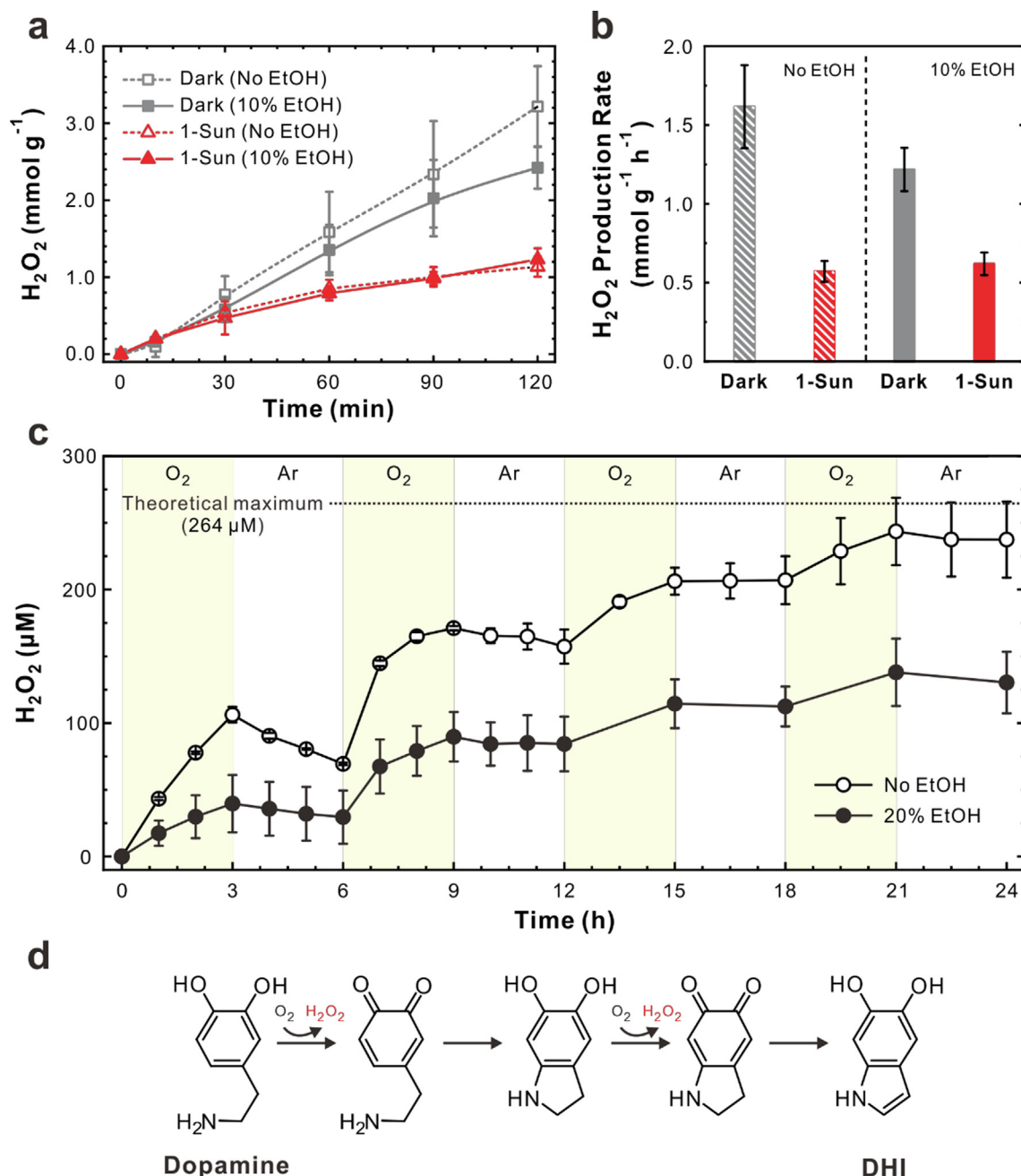


Fig. 1. Chemical production of H_2O_2 by dopamine. (a) Time-dependent profiles of H_2O_2 production by dopamine. (b) Comparison of the H_2O_2 production rate by dopamine in the presence and absence of ethanol under light irradiation and dark for 2 h. (c) Time-dependent profiles of H_2O_2 production by dopamine in the presence and absence of ethanol with alternating O_2 and Ar gas purging for 24 h. (d) Chemical auto-oxidation pathway of dopamine for the production of H_2O_2 . Experimental conditions: [dopamine] = $25.1\ mg\ L^{-1}$, $pH_i = 6$, [EtOH] $_0 = 0, 10,$ and $20\ vol\%$ as an electron donor and O_2 -saturated. Multiple experiments were independently conducted at least three times.

groups by ethanol, as observed in the UV/vis absorption spectra (Fig. S1), thus resulting in the operation of only one ORR process. These results collectively indicate that the production of H_2O_2 using dopamine originates from the chemical conversion by the multistep oxidation pathways involving various oxidized forms of dopamine (Fig. 1d and Scheme S1).

The effects of pH and ion concentration on the performance of dopamine for the production of H_2O_2 was examined in various acids (e.g., $HClO_4$, HCl , and H_2SO_4) at pH 3 (Fig. S3a) and in various concentrations of phosphate-buffered saline (PBS) solution at pH 6 (Fig. S3b). We found that the activity decreased markedly upon increasing the concentration of protons regardless of the type of

acid ($1.608\ mmol\ g^{-1}\ h^{-1}$ at pH 6 to $0.0034\ mmol\ g^{-1}\ h^{-1}$ at pH 3) and buffer ions ($1.608\ mmol\ g^{-1}\ h^{-1}$ in 0 mM PBS to $0.00727\ mmol\ g^{-1}\ h^{-1}$ in 100 mM PBS). It indicates that these supporting ions also interfere with the chemical self-oxidation of dopamine, thus resulting in a decrease in the amount of H_2O_2 generated [37,38].

To further elucidate the role of the chemical moiety present in dopamine, the performance of various dopamine derivatives such as 3,4-dimethoxyphenylethylamine (PEA), 3,4-dihydroxyphenyl propanoic acid (PPA), indole, and 5,6-dihydroxyindole (DHI), for the production of H_2O_2 was investigated in the dark under O_2 saturation (Fig. 2). These structural differences resulted in a lack of catalytic activity for the production of H_2O_2 , indicating that both

catechol and amine groups are essential for the spontaneous oxidation of dopamine with O_2 . Furthermore, slight formation of H_2O_2 was observed for DHI, whereas negligible activity was detected for indole. These results strongly imply that the co-existence of both catechol and primary amine groups is critical for the chemical auto-oxidation of dopamine and the subsequent generation of H_2O_2 induced by two-electron ORR.

3.2. Characterizations of PDA

We then synthesized PDA following previous reports under basic conditions to compare the catalytic performance of PDA derived from dopamine with that of dopamine [39]. Briefly, DHI—spontaneously generated by a series of oxidation steps from dopamine—is a widely accepted predominant building block for self-polymerized PDA [40,41]. Since the pK_{a1} and pK_{a2} value for the catechol groups of dopamine is approximately 9.25 and 13 respectively, the hydroxyl group is deprotonated under basic conditions, and neighboring oxygen accepts an electron to produce the catechol-quinone complex [42]. Subsequently, the complex reacts with either dopamine or DHI to form PDA through the dopamine-quinone formation. For the H_2O_2 generation, the reaction time and pH condition were optimized to 30 h and pH 11, respectively, to enable the synthesis of uniform and well-dispersed spherical PDA particles (Fig. S4 and S5). The resulting scanning electron microscopy (SEM) with energy-dispersive X-ray spectroscopy (EDX) mapping images confirmed the successful formation of spherical PDA particles with an average diameter of 231 ± 21 nm without noticeable observation of aggregated structures (Fig. 3a,b, and S4).

Although the present heterogeneity in a monomeric unit has made it difficult to understand the details regarding the PDA structures and its polymerization mechanism [30,41], we attempted to determine the detailed chemical structures of PDA using X-ray photoelectron spectroscopy (XPS, Fig. 3c) and solid-state ^{13}C NMR spectroscopy (Fig. 3d). Specifically, PDA mainly consisted of carbon (75.1 at.%) and oxygen (16.9 at.%), with a distinct evolution of the nitrogen peak at approximately 7.94 at.%. The peaks observed at 31 and 45 ppm in ^{13}C NMR spectra are assigned to carbons *h* and *g*, respectively, (Fig. 3d,e), which are partially saturated five-membered ring or aminoethyl moieties in non-cyclized units. The peaks at 161 and 175 ppm are assigned to the two oxygen-bound carbons (*b* and *a*) due to the high downfield shift commonly observed in deshielded moieties. The signals observed in the range from 100 to 150 ppm correspond to the carbon centres in the cyclic core of PDA. Among them, the most downfield signal at 145 ppm is attributed to the carbon atom *f* (Fig. 3d,e), adjacent to the nitrogen atom. The characteristic peak at 119 ppm can be assigned to quaternary carbon atoms in benzo positions *c* and *d* (Fig. 3d,e) at the bridging points between monomer units. A small shoulder peak was observed at approximately 100 ppm, which could be attributed to the resonance structure of PDA; it can be assigned to benzylic carbon and the pyrrole ring of indoles (*g'* and *h'* in Fig. 3d,e).

Moreover, the optical properties and electronic structure of PDA were investigated using UV/vis spectroscopy (Fig. 3f) and ultraviolet photoelectron spectroscopy (UPS) (Fig. 3g). As shown in Fig. S1, the absorption spectrum of dopamine exhibits a prominent peak at ~ 280 nm; it is attributed to the $\pi-\pi^*$ transition of the benzene ring. After polymerization, the spectrum of PDA exhibits broad absorption peaks from 300 to 600 nm, implying that PDA can utilize a broad range of light effectively. According to the Tauc plot of PDA, the indirect band gap of PDA was determined to be 1.93 eV (Fig. 3f) and direct band gap was 2.53 eV (Fig. S6), which were similar to previous [43,44]. However, dopamine possesses a comparatively high band gap of 4.09 eV (Fig. S7). The band structure of PDA is proposed based on the valence band measurement using UPS

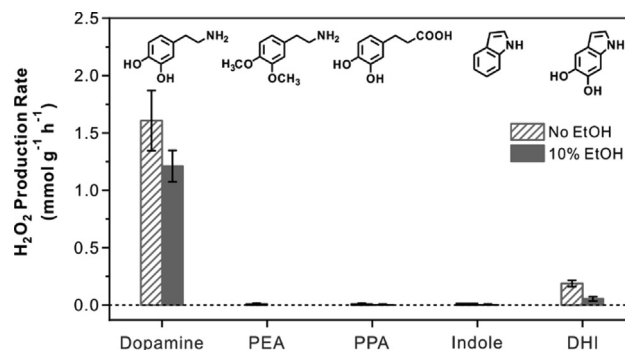


Fig. 2. H_2O_2 production rates of various dopamine derivatives. Samples include dopamine, 3,4-dimethoxyphenyl ethylamine (PEA), 3,4-dihydroxyphenyl propanoic acid (PPA), indole, and 5,6-dihydroxyindole (DHI) under dark conditions for 2 h. The experimental conditions were as follows: [chemicals] = 25.1 mg L⁻¹, [EtOH]₀ = 0 or 10 vol% (as an electron donor), O_2 -saturated. Multiple experiments were conducted at least two times independently.

(Fig. 3g), as shown in Fig. 3h; this band structure is suitable for H_2O_2 generation (conduction band of -4.04 eV and valence band of -5.97 eV), enabling two-electron reduction of O_2 to H_2O_2 . These results strongly imply that semiconducting PDA can exhibit a photo-responsive behavior and photocatalytic H_2O_2 production, in contrast to the chemical production of H_2O_2 by dopamine via a self-oxidation process.

3.3. Photocatalytic H_2O_2 production of PDA

The photocatalytic activity of PDA for producing H_2O_2 was then evaluated under solar-simulated light (1-sun) and visible light (≥ 420 nm) illumination in the presence or absence of ethanol and oxygen (Fig. 4). To compare performance more clearly, the photocatalytic activity of PDA was examined under identical conditions with dopamine. PDA exhibited a maximum H_2O_2 yield of 0.531 mmol g⁻¹ h⁻¹ under light irradiation with ethanol as the electron donor, and a high H_2O_2 yield of 0.247 mmol g⁻¹ h⁻¹ was also achieved even with irradiation by visible light (≥ 420 nm) (Fig. 4a,b). Furthermore, the generation of H_2O_2 using PDA in the absence of ethanol was significantly high (0.451 mmol g⁻¹ h⁻¹), which was approximately 85% of its performance in the absence of 10 vol% ethanol (0.531 mmol g⁻¹ h⁻¹). However, PDA showcased a negligible photocatalytic performance for H_2O_2 generation in the absence of light (0.0307 mmol g⁻¹ h⁻¹) and O_2 sources (0.0178 mmol g⁻¹ h⁻¹), demonstrating that both light and oxygen are essential for the production of H_2O_2 by PDA, as the production is achieved via photo-responsive catalytic ORR. In addition to results revealing the insignificant water-splitting capability of PDA (Table S2), this observation indicates that H_2O_2 is not produced via water oxidation reaction using photoexcited holes. In contrast, it originates from the reduction reaction of generated electrons with O_2 . Additionally, apparent quantum yield (AQY) of PDA was measured as a function of the incident light wavelength (Fig. 4c). The obtained AQY spectrum of PDA has a similar spectral profile to its absorbance spectrum, clearly demonstrating that the production of H_2O_2 is a result of the photocatalytic ORR by PDA.

To clarify the catalytic performance of PDA, the photoelectrochemical analysis with CV and EIS of PDA were performed in PBS (0.10 M, pH 7) electrolyte (Fig. S8). The current of PDA was enhanced under O_2 saturation, which was more increased under irradiation, supporting that the PDA represented catalytic activity for both photon and O_2 . As shown in Fig. S8, the resistance of PDA under O_2 and irradiation (0.32 k Ω) is significantly lower than that of PDA under dark in presence of Ar (10.1 k Ω) and O_2 (0.36 k Ω), indicating that PDA has photoelectrochemical activity that is

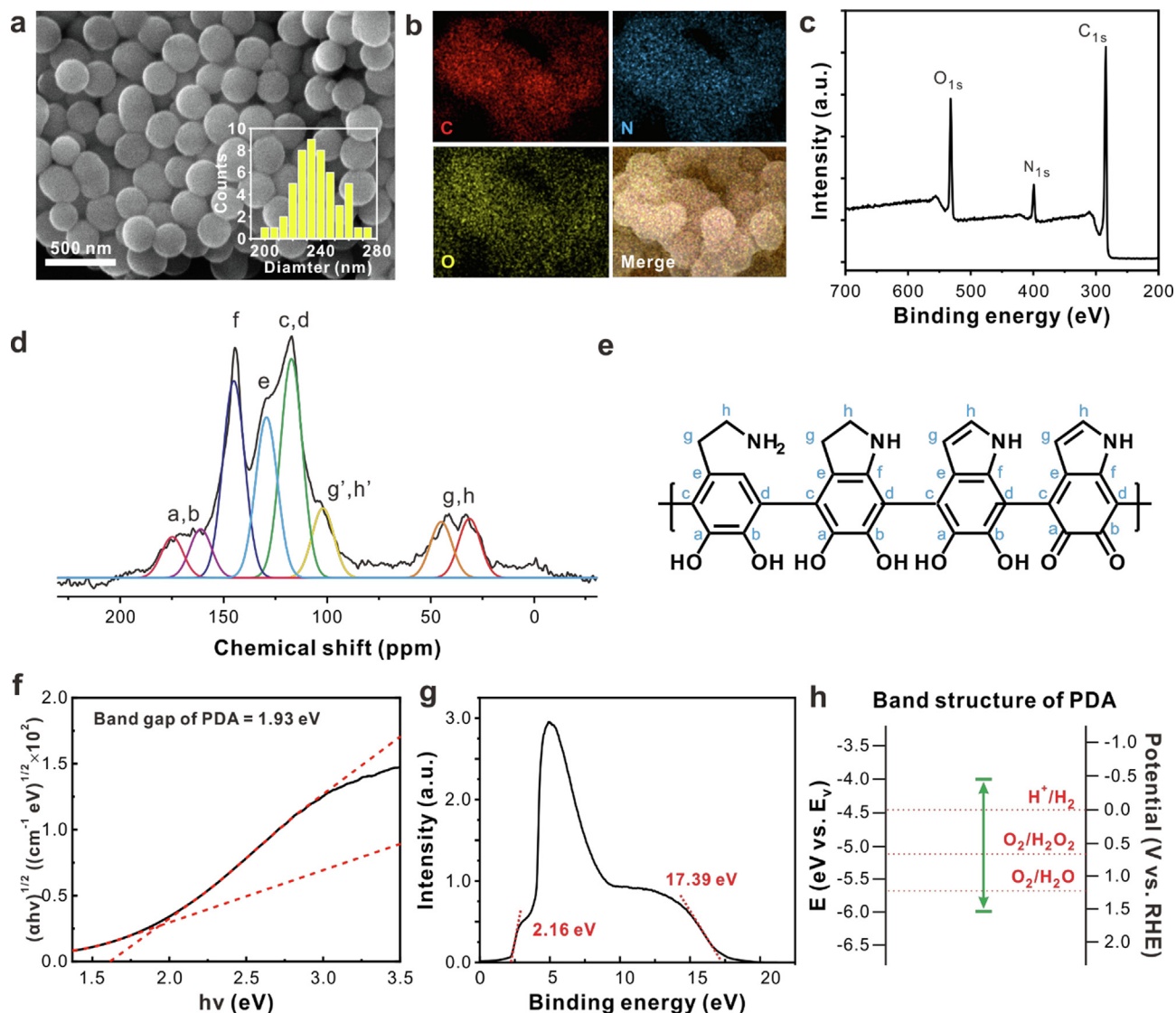


Fig. 3. Structural and chemical characterizations of PDA. (a) Representative SEM image of PDA with a corresponding size distribution histogram. (b) EDX mapping images of PDA with carbon, nitrogen, oxygen, and merged, respectively. (c) XPS survey spectrum of PDA. (d) Solid-state ^{13}C NMR spectra of PDA recorded at a MAS frequency of 12 kHz using the standard cross-polarization-magic angle spinning (CP-MAS) sequence. (e) Chemical structure of PDA with the assigned chemical shift in solid-state ^{13}C NMR. (f) Band gap evaluation of PDA using a Tauc plot. (g) UPS survey spectra of PDA. (h) Schematic band structure of PDA.

enhanced by O_2 . Additionally, to analyze the selectivity for 2-electron ORR, we measured RRDE and calculated the selectivity in Fig. S9. As shown in the figure, as the rotation rate meaning O_2 diffusion rate increases, the ring and disk current increases exhibiting electrocatalytic activity of PDA for H_2O_2 productivity (Fig. S9a). The RRDE experiments showed that PDA produces H_2O_2 with up to 78 % selectivity and the ORR on PDA mainly via an adjacent 2-electron pathway ($n = 2.5$) (Fig. S9b). This result supports that PDA has efficient selectivity for electrocatalytic H_2O_2 production.

The amount of photochemically produced H_2O_2 was monitored under various pH conditions (Fig. S10a). It was found that the photocatalytic activity decreases under more acidic conditions with a minimum activity of $0.20 \text{ mmol g}^{-1}\text{h}^{-1}$ at pH 1. In contrast, the photocatalytic activity gradually increases under alkaline conditions, with a maximum value of $1.70 \text{ mmol g}^{-1}\text{h}^{-1}$ at pH 12. According to a previous study, the accelerating production rate of photocatalytic H_2 is proportional to the increase in pH because the oxidation potential of sacrificial electron donors (e.g., ethanol) shifts cathodically with an increase in pH [45]. In this study, we

also observed that PDA underwent a greater degree of agglomeration under acidic conditions; hence, it results in poor dispersibility and reduced catalytic activity (Fig. S10b). However, it was recovered to the original level of dispersibility by shifting pH toward the alkaline region (e.g., pH 12). It is worth noting that this pH-dependent dispersibility of PDA can be highly useful for the simple and easy collection of heterogeneous photocatalysts via alternating pH as a perspective on sustainable and recyclable catalytic performance.

While the exact monomeric units of the PDA are still elusive, we verified the contribution of the structural unit to the photocatalytic activity using molecular analogues, PEA, PPA, indole, and DHI, to monitor the generation of H_2O_2 under light irradiation (Fig. 4d). For example, PPA exhibited a low activity ($0.0750 \text{ mmol g}^{-1}\text{h}^{-1}$ in the absence of ethanol and $0.00973 \text{ mmol g}^{-1}\text{h}^{-1}$ in the presence of ethanol) for the production of H_2O_2 under light irradiation, while PEA showed a higher photocatalytic yield ($0.249 \text{ mmol g}^{-1}\text{h}^{-1}$ in the absence of ethanol, and $0.157 \text{ mmol g}^{-1}\text{h}^{-1}$ in the presence of ethanol) than PPA. To our surprise, DHI ($0.244 \text{ mmol g}^{-1}\text{h}^{-1}$ in the absence of ethanol and $0.300 \text{ mmol g}^{-1}\text{h}^{-1}$ in the presence of

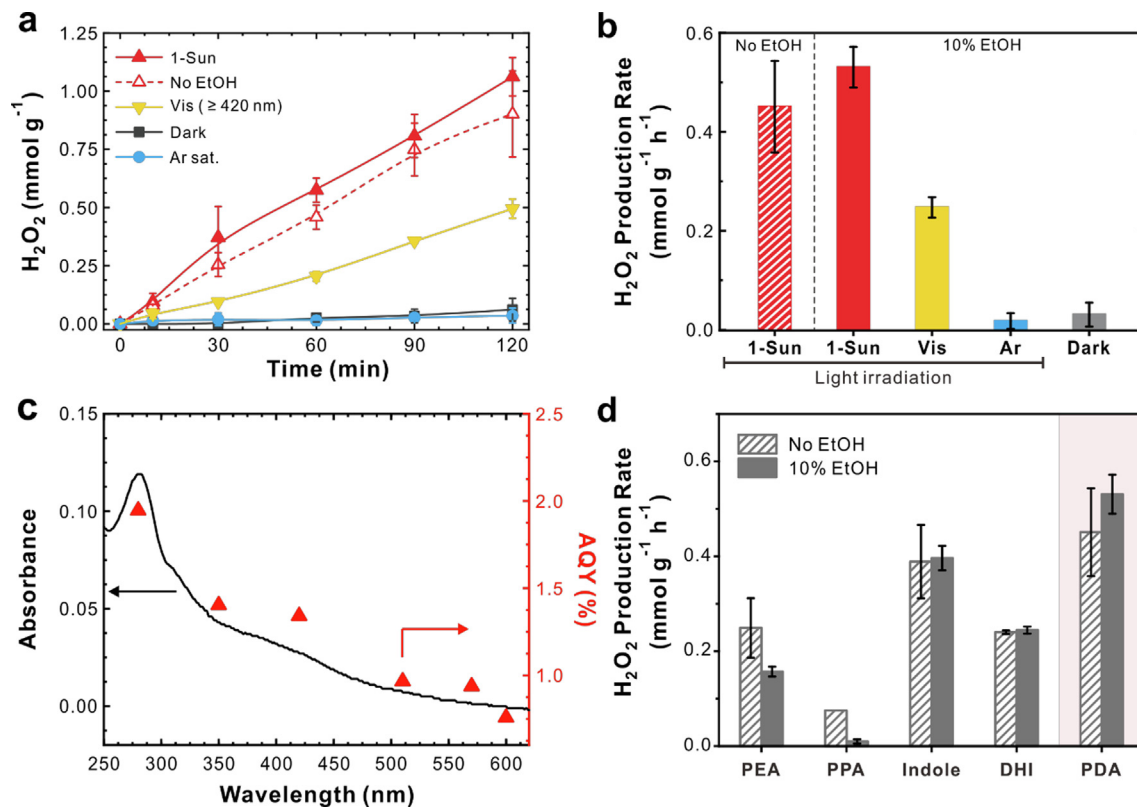


Fig. 4. Photocatalytic production of H₂O₂ by PDA. (a) Time-dependent profiles and (b) corresponding rates of H₂O₂ production by PDA over 2 h in the absence of ethanol (under light irradiation), in the presence of ethanol (under light irradiation), under visible light irradiation (≥420 nm, with ethanol), under Ar saturation (with ethanol and under light irradiation), and in the dark (with ethanol). (c) Absorbance spectrum (black) and apparent quantum yield (AQY, red) of the photocatalytic H₂O₂ production in various wavelengths for PDA. (d) H₂O₂ production rates of PEA, PPA, indole, DHI, and PDA under light irradiation. The experimental default conditions were as follows: [catalyst or chemical] = 25.1 mg L⁻¹, pH_i = 6, 100 mW cm⁻² (AM 1.5), [EtOH]₀ = 10 vol% (as an electron donor), O₂-saturated, and for 2 h. Multiple experiments were independently conducted at least three times.

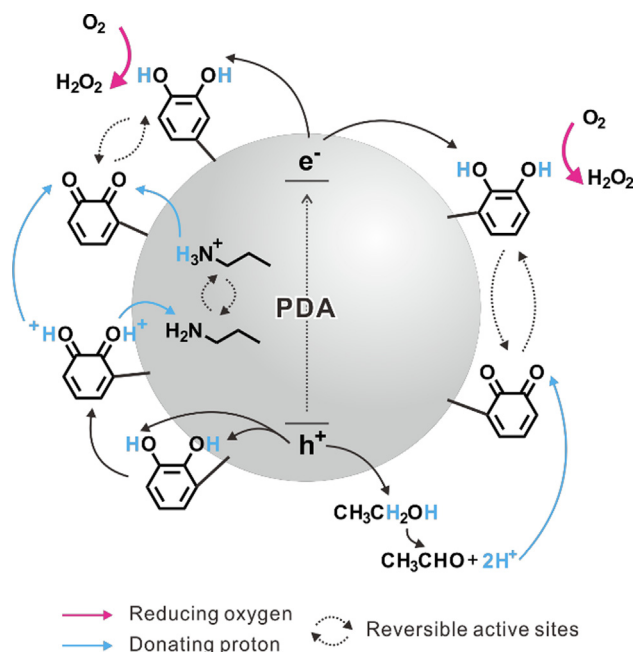
ethanol) and indole (0.389 mmol g⁻¹h⁻¹ in the absence of ethanol and 0.396 mmol g⁻¹h⁻¹ in the presence of ethanol) both exhibited remarkably high H₂O₂ generation rates—comparable to that of PDA—as major unit structures of PDA, implying that both indole and catechol moieties play a critical role in the photocatalytic generation of H₂O₂.

Therefore, we further analyzed the chemical transformation in the indole group under light irradiation by liquid chromatography-mass spectrometry (LC-MS) before and after photocatalytic reactions (Fig. S11). A new major peak was observed at 148 *m/z* after the photocatalytic reaction besides the peak of indole at 118 *m/z*, corresponding to the isatin structure as an oxidized form of indole. In an indole structure without catechol groups, light irradiation can induce radicals on nitrogen atoms. Thereafter, O₂ can easily interact with the relatively electron-deficient carbon atoms adjacent to nitrogen, resulting in the formation of isatin and the production of H₂O₂. The H₂O₂ production rate using isatin as a starting catalyst, which is not transformed from indole, is relatively too low both in the presence and absence of ethanol under light irradiation (Fig. S12). It is because the isatin is a totally oxidized form, like benzoquinone, making it hard to directly reduce O₂ under mild conditions, excluding metal catalysts or organic solvents [46]. This indicates that the high H₂O₂ production achieved by indole could be mainly attributed to a photoinduced structure-transforming process from indole to isatin by consuming O₂.

Based on these results, we propose a possible mechanism for photocatalytic H₂O₂ production on the surface of PDA (Scheme 2

and Scheme S2). As a primary reaction in PDA, photoexcited electrons were transferred to the catechol groups of PDA upon light irradiation. Subsequently, oxygen was reduced to H₂O₂ by consuming photoexcited electrons and protons originating from catechol groups. These steps were accompanied by the conversion of the catechol groups to 1,2-benzoquinone groups. Simultaneously, photoexcited holes reacted with hydroxyl groups of the catechol moiety on PDA to form carbonyl groups and with ethanol, releasing a couple of protons. In addition to the photochemically formed protons, the protons from the protonated amine (–NH₃⁺) groups can be donated to adjacent carbonyl and 1,2-benzoquinone groups, resulting in a recovery of hydroxyl and catechol groups as active sites for H₂O₂ production. Another minor pathway for H₂O₂ production is also possible via the oxidation of the indole group on the surface of PDA, as shown in Scheme S2.

We investigate the long-term performance of PDA to generate H₂O₂ under alternating light irradiation conditions to evaluate its stability as a sustainable photocatalyst (Fig. 5a,b). PDA exhibited photoresponsivity with excellent activity retention of ~90% over four repeated cycles. In contrast, the performance of dopamine and DHI decreased gradually with low activity retention of ~40 and ~20%, respectively (Fig. S13). This can be explained by the reversible photocatalytic reaction of PDA as a light-absorbing semiconductor; however, PDA has a structure similar to those of dopamine and DHI. The generation of H₂O₂ by dopamine occurred via a chemical oxidation reaction by changing the chemical structure and increasing the concentration of the oxidized forms of dopamine, such as DHI, as shown in Fig. 1d. Interestingly, however,



no significant changes in the structure of PDA were observed in the UV/vis absorbance spectra (Fig. S14) and the characteristic solid-state ¹³C NMR signals of PDA during the photocatalytic reaction (Fig. S15 and Table S3), indicating the excellent durability and reproducibility of PDA under the reaction conditions. This result

was also consistent with the XPS spectra (Fig. S16), in which the intensity and binding energy observed for PDA remained relatively constant, even after the photocatalytic ORR.

PDA, which is inspired by the adhesive nature of catechol and amine in mussel proteins, is one of the simplest and most versatile materials for surface engineering. Hence, PDA can be coated on virtually any type of material surface, including metals, metal oxide semiconductors, ceramics, and polymers. As a result, it has been widely used in various surface chemistry and applications [40,47]. In this study, owing to the excellent adhesive nature of PDA, we fabricated heterogeneous photocatalytic films for H₂O₂ production by uniformly coating PDA onto diverse substrates (without any pretreatment), including Ni foam, graphite foil, Ti foil, glass, and polyethylene terephthalate (PET); we also investigated the photocatalytic performance of these materials (Fig. 5c,d). All the PDA-coated substrates displayed outstanding photocatalytic performance in the production of H₂O₂ for 2 h (more than 4.07 μM cm⁻²), with the highest performance on the Ni foam substrate (35.2 μM cm⁻²) due to the porous structure of Ni foam. The outstanding photocatalytic performance of PDA film based on its exceptional surface adhesion ability renders it both environmentally and economically applicable in the sustainable production of H₂O₂ compared to other conventional photocatalyst films with poor adhesive property on glass substrates (e.g., C₃N₄, see Fig. S17).

4. Conclusions

We demonstrate dopamine-based novel green and sustainable production of H₂O₂. The proposed H₂O₂ production by dopamine represents different oxygen reduction mechanisms, changing from a chemical process to a photocatalytic process by structural transformation of dopamine to DHI and PDA. During the auto-oxidation of dopamine, which involved the transition of catechol to hydroquinone groups and the ring closure of the amine group, H₂O₂

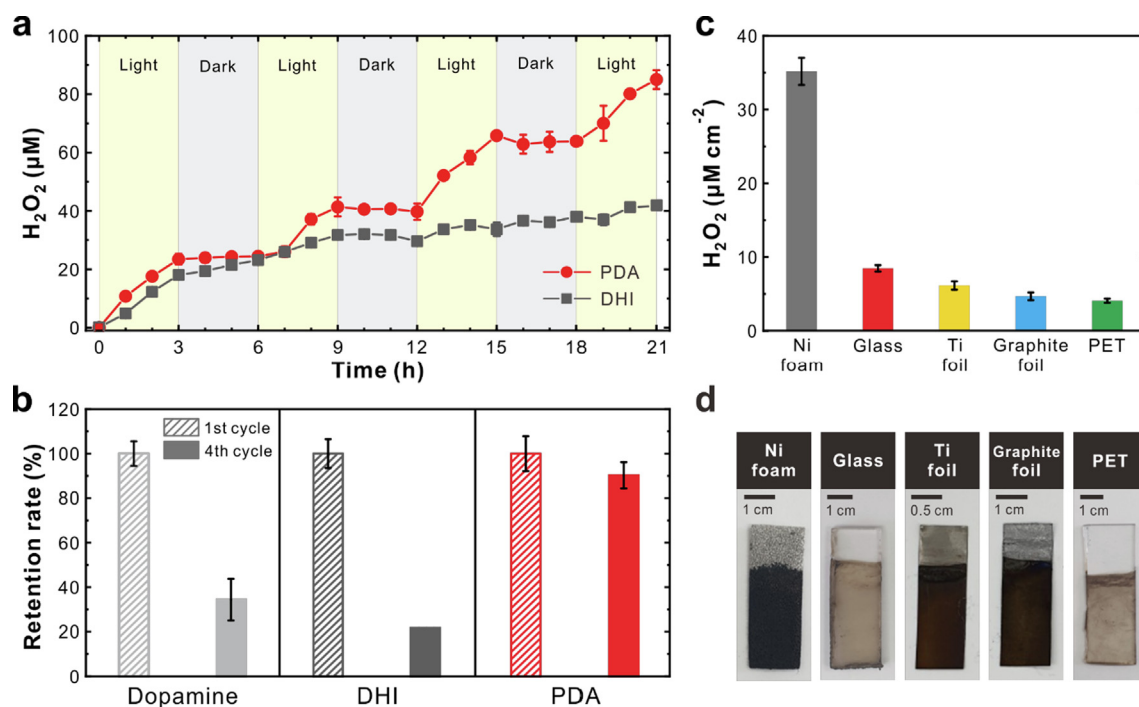


Fig. 5. Versatility of heterogeneous PDA photocatalysts. (a) Time-dependent of H₂O₂ production of PDA or DHI with/without light irradiation each for 3 h. (b) Performance retention of the 1st and 4th cycles of dopamine with alternating O₂ and Ar condition under dark for chemical production. DHI and PDA with alternating light and dark conditions under O₂ saturation for photocatalytic production. (c) Photocatalytic H₂O₂ performance test for 2 h. (d) Photographic images of various substrates (graphite foil, Ni foam, Ti foil, glass, and PET) coated with PDA. The experimental default conditions were as follows: [PDA, DHI, or dopamine] = 25.1 mg L⁻¹, 100 mW cm⁻² (AM 1.5), [EtOH]₀ = 0 vol% (for Fig. 5a,b) and 10 vol% (for Fig. 5c,d) (as an electron donor), and O₂-saturated. Multiple experiments were independently conducted at least three times.

was chemically generated without an extra electron donor and additional energy sources. In contrast, PDA exhibited excellent photocatalytic activity in producing H_2O_2 , with a reversible reaction occurring between the catechol and 1,2-benzoquinone groups of PDA. Notably, PDA showed a considerable H_2O_2 production rate in the absence of additional electron donors owing to its unique self-electron-donating abilities, which was achieved by utilizing its diverse surface functional groups, such as hydroxyl and amine groups. Furthermore, the pH-dependent dispersibility and versatile adhesion ability of PDA make it useful as a recyclable heterogeneous photocatalyst and in surface engineering applications regardless of substrate type. We anticipate that these unique properties of dopamine will offer a new strategy for H_2O_2 production using dopamine that will facilitate the design of environmentally friendly and sustainable green catalysts to achieve high solar-to- H_2O_2 conversion performance.

Declaration of Competing Interest

The authors declare that they have no known competing financial interests or personal relationships that could have appeared to influence the work reported in this paper.

Acknowledgments

We thank Dr. Eeseul Shin for initial help and comments on the project. This work was supported by the National Research Foundation of Korea (NRF-2021R1F1A1063702, NRF-2021R1A2C3004978, NRF-2018R1A5A1025208, NRF-2017M3A7B4052802, and NRF-2021R1C1C1007706), and by the Ecological Imitation-based Environmental Pollution Management Technology Development Project (2019002790008) funded by the Korea Ministry of Environment (MOE).

Appendix A. Supplementary material

Detailed characterizations including UV/vis spectra, SEM, and AFM images, LC-MS, solid state-NMR, XPS, photocatalytic performance at various pH, and additional scheme, Figures, and tables (PDF).

Supplementary data to this article can be found online at <https://doi.org/10.1016/j.jcat.2022.05.017>.

References

- I. Oller, S. Malato, J.A. Sánchez-Pérez, Combination of advanced oxidation processes and biological treatments for wastewater decontamination—a review, *Sci. Total Environ.* 409 (20) (2011) 4141–4166.
- K. Kamata, K. Yonehara, Y. Sumida, K. Yamaguchi, S. Hikichi, N. Mizuno, Efficient epoxidation of olefins with $\geq 99\%$ selectivity and use of hydrogen peroxide, *Science* 300 (2003) 964.
- S. Fukuzumi, Y. Yamada, K.D. Karlin, Hydrogen peroxide as a sustainable energy carrier: electrocatalytic production of hydrogen peroxide and the fuel cell, *Electrochim. Acta* 82 (2012) 493–511.
- A.R. Bowers, P. Gaddipati, W.W. Eckenfelder, R.M. Monsen, Treatment of toxic or refractory wastewaters with hydrogen peroxide, *Water Sci. Technol.* 21 (6–7) (1989) 477–486.
- D. Hâncu, J. Green, E.J. Beckman, H_2O_2 in CO_2/H_2O biphasic systems: green synthesis and epoxidation reactions, *Ind. Eng. Chem.* 41 (2002) 4466–4474.
- J.M. Campos-Martin, G. Blanco-Brieva, J.L.G. Fierro, Hydrogen peroxide synthesis: an outlook beyond the anthraquinone process, *Angew. Chem. Int. Ed.* 45 (42) (2006) 6962–6984.
- Y. Nosaka, A.Y. Nosaka, Generation and detection of reactive oxygen species in photocatalysis, *Chem. Rev.* 117 (17) (2017) 11302–11336.
- Y. Kofuji, Y. Isobe, Y. Shiraishi, H. Sakamoto, S. Tanaka, S. Ichikawa, T. Hirai, Carbon nitride–aromatic diimide–graphene nanohybrids: metal-free photocatalysts for solar-to-hydrogen peroxide energy conversion with 0.2% efficiency, *J. Am. Chem. Soc.* 138 (2016) 10019–10025.
- M. Gu, D.-Y. Lee, J. Mun, D. Kim, H.-I. Cho, B. Kim, W. Kim, G. Lee, B.-S. Kim, H.-I. Kim, Solar-to-hydrogen peroxide conversion of photocatalytic carbon dots with anthraquinone: unveiling the dual role of surface functionalities, *Appl. Catal. B* 312 (2022) 121379.
- Z. Teng, Q. Zhang, H. Yang, K. Kato, W. Yang, Y.-R. Lu, S. Liu, C. Wang, A. Yamakata, C. Su, B. Liu, T. Ohno, Atomically dispersed antimony on carbon nitride for the artificial photosynthesis of hydrogen peroxide, *Nat. Catal.* 4 (5) (2021) 374–384.
- Y. Shiraishi, S. Kanazawa, Y. Kofuji, H. Sakamoto, S. Ichikawa, S. Tanaka, T. Hirai, Sunlight-driven hydrogen peroxide production from water and molecular oxygen by metal-free photocatalysts, *Angew. Chem. Int. Ed.* 53 (49) (2014) 13454–13459.
- X. Dong, F. Cheng, Recent development in exfoliated two-dimensional $g-C_3N_4$ nanosheets for photocatalytic applications, *J. Mater. Chem. A* 3 (47) (2015) 23642–23652.
- M. Gryszel, M. Sytnyk, M. Jakešová, G. Romanazzi, R. Gabriellson, W. Heiss, E.D. Glowacki, General observation of photocatalytic oxygen reduction to hydrogen peroxide by organic semiconductor thin films and colloidal crystals, *ACS Appl. Mater. Interfaces* 10 (16) (2018) 13253–13257.
- E. Miglbauer, M. Gryszel, E.D. Glowacki, Photochemical evolution of hydrogen peroxide on lignins, *Green Chem.* 22 (3) (2020) 673–677.
- M. Jakešová, D.H. Apaydin, M. Sytnyk, K. Oppelt, W. Heiss, N.S. Sariciftci, E.D. Glowacki, Hydrogen-bonded organic semiconductors as stable photoelectrocatalysts for efficient hydrogen peroxide photosynthesis, *Adv. Funct. Mater.* 26 (29) (2016) 5248–5254.
- W. Fan, B. Zhang, X. Wang, W. Ma, D. Li, Z. Wang, M. Dupuis, J. Shi, S. Liao, C. Li, Efficient hydrogen peroxide synthesis by metal-free polyterthiophene via photoelectrocatalytic dioxygen reduction, *Energy Environ. Sci.* 13 (1) (2020) 238–245.
- L. Migliaccio, M. Gryszel, V. Derek, A. Pezzella, E.D. Glowacki, Aqueous photo (electro)catalysis with eumelanin thin films, *Mater. Horiz.* 5 (5) (2018) 984–990.
- Y. Shiraishi, T. Takii, T. Hagi, S. Mori, Y. Kofuji, Y. Kitagawa, S. Tanaka, S. Ichikawa, T. Hirai, Resorcinol–formaldehyde resins as metal-free semiconductor photocatalysts for solar-to-hydrogen peroxide energy conversion, *Nat. Mater.* 18 (9) (2019) 985–993.
- P. Muñoz, S. Huenchuguala, I. Paris, J. Segura-Aguilar, Dopamine oxidation and autophagy, *Parkinsons Dis.* 2012 (2012) 920953.
- Q. Wei, F. Zhang, J. Li, B. Li, C. Zhao, Oxidant-induced dopamine polymerization for multifunctional coatings, *Polym. Chem.* 1 (9) (2010) 1430, <https://doi.org/10.1039/c0py00215a>.
- V. Ball, D. Del Frari, M. Michel, M.J. Buehler, V. Toniazio, M.K. Singh, J. Gracio, D. Ruch, Deposition mechanism and properties of thin polydopamine films for high added value applications in surface science at the nanoscale, *Bionanoscience* 2 (1) (2012) 16–34.
- M. D'Ischia, A. Napolitano, V. Ball, C.-T. Chen, M.J. Buehler, Polydopamine and eumelanin: from structure–property relationships to a unified tailoring strategy, *Acc. Chem. Res.* 47 (2014) 3541–3550.
- H.J. Cox, J. Li, P. Saini, J.R. Paterson, G.J. Sharples, J.P.S. Badyal, Bioinspired and eco-friendly high efficacy cinnamaldehyde antibacterial surfaces, *J. Mater. Chem. B* 9 (12) (2021) 2918–2930.
- W.-X. Mao, X.-J. Lin, W. Zhang, Z.-X. Chi, R.-W. Lyu, A.-M. Cao, L.-J. Wan, Core-shell structured TiO_2 @polydopamine for highly active visible-light photocatalysis, *Chem. Commun.* 52 (44) (2016) 7122–7125.
- H.J. Nam, B. Kim, M.J. Ko, M. Jin, J.M. Kim, D.-Y. Jung, A new mussel-inspired polydopamine sensitizer for dye-sensitized solar cells: controlled synthesis and charge transfer, *Chem. Eur. J.* 18 (2012) 14000–14007.
- S. Mei, X. Xu, R.D. Priestley, Y. Lu, Polydopamine-based nanoreactors: synthesis and applications in bioscience and energy materials, *Chem. Sci.* 11 (2020) 12269–12281.
- P. Makuła, M. Pacia, W. Macyk, How to correctly determine the band gap energy of modified semiconductor photocatalysts based on UV–Vis spectra, *J. Phys. Chem. Lett.* 9 (23) (2018) 6814–6817.
- H. Bader, V. Sturzenegger, J. Hoigné, Photometric method for the determination of low concentrations of hydrogen peroxide by the peroxidase catalyzed oxidation of N, N-diethyl-p-phenylenediamine (DPD), *Water Res.* 22 (9) (1988) 1109–1115.
- Y. Choi, G.H. Ryu, S.H. Min, B.R. Lee, M.H. Song, Z. Lee, B.-S. Kim, Interface-controlled synthesis of heterodimeric silver–carbon nanoparticles derived from polysaccharides, *ACS Nano* 8 (11) (2014) 11377–11385.
- D.R. Dreyer, D.J. Miller, B.D. Freeman, D.R. Paul, C.W. Bielawski, Elucidating the structure of poly(dopamine), *Langmuir* 28 (15) (2012) 6428–6435.
- S. Ben Aoun, Nanostructured carbon electrode modified with N-doped graphene quantum dots–chitosan nanocomposite: a sensitive electrochemical dopamine sensor, *R. Soc. Open Sci.* 4 (2017) 171199.
- X. Han, F. Tang, Z. Jin, Free-standing polydopamine films generated in the presence of different metallic ions: the comparison of reaction process and film properties, *RSC Adv.* 8 (2018) 18347–18354.
- M. Salomäki, L. Marttila, H. Kivela, T. Ouvinen, J. Lukkari, Effects of pH and oxidants on the first steps of polydopamine formation: a thermodynamic approach, *J. Phys. Chem.* 122 (2018) 6314–6327.
- S.-M. Chen, J.-Y. Chen, V.S. Vasantha, Electrochemical preparation of epinephrine/Nafion chemically modified electrodes and their electrocatalytic oxidation of ascorbic acid and dopamine, *Electrochim. Acta* 52 (2) (2006) 455–465.
- A. Daniel Arulraj, A. Arunkumar, M. Vijayan, K. Balaji Viswanath, V.S. Vasantha, A simple route to develop highly porous nano polypyrrole/reduced graphene oxide composite film for selective determination of dopamine, *Electrochim. Acta* 206 (2016) 77–85.
- S. Palanisamy, B. Thirumalraj, S.-M. Chen, M. Ajmal Ali, K. Muthupandi, R. Emmanuel, P. Prakash, F.M.A. Al-Hemaid, Fabrication of silver nanoparticles

- decorated on activated screen printed carbon electrode and its application for ultrasensitive detection of dopamine, *Electroanalysis* 27 (8) (2015) 1998–2006.
- [37] S. Chuekchang, S. Chaiyasit, V. Kruefu, S. Phanichphant, in: 2010 IEEE 5th International Conference on Nano/Micro Engineered and Molecular Systems, 2010, pp. 133–137.
- [38] I. Zmerli, J.-P. Michel, A. Makky, Bioinspired polydopamine nanoparticles: synthesis, nanomechanical properties, and efficient PEGylation strategy, *J. Mater. Chem. B* 8 (2020) 4489–4504.
- [39] E.K. Jeon, E. Seo, E. Lee, W. Lee, M.-K. Um, B.-S. Kim, Mussel-inspired green synthesis of silver nanoparticles on graphene oxide nanosheets for enhanced catalytic applications, *Chem. Commun.* 49 (33) (2013) 3392, <https://doi.org/10.1039/c3cc00115f>.
- [40] H. Lee, S.M. Dellatore, W.M. Miller, P.B. Messersmith, Mussel-inspired surface chemistry for multifunctional coatings, *Science* 318 (5849) (2007) 426–430.
- [41] J. Liebscher, R. Mrówczyński, H.A. Scheidt, C. Filip, N.D. Hädade, R. Turcu, A. Bende, S. Beck, Structure of polydopamine: a never-ending story?, *Langmuir* 29 (2013) 10539–10548.
- [42] J.A. Dean, Lange's handbook of chemistry, *Mater. Manuf. Process* 5 (4) (1990) 687–688.
- [43] S. Kim, G.-H. Moon, G. Kim, U. Kang, H. Park, W. Choi, TiO₂ complexed with dopamine-derived polymers and the visible light photocatalytic activities for water pollutants, *J. Catal.* 346 (2017) 92–100.
- [44] J. Tripathy, G. Loget, M. Altomare, P. Schmuki, Polydopamine-coated TiO₂ nanotubes for selective photocatalytic oxidation of benzyl alcohol to benzaldehyde under visible light, *J. Nanosci. Nanotechnol.* 16 (2016) 5353–5358.
- [45] P.o. Wu, J. Wang, J. Zhao, L. Guo, F.E. Osterloh, High alkalinity boosts visible light driven H₂ evolution activity of g-C₃N₄ in aqueous methanol, *Chem. Commun.* 50 (98) (2014) 15521–15524.
- [46] S. Varun, R. Kakkar, Isatin and its derivatives: a survey of recent syntheses, reactions, and applications, *Medchemcomm.* 10 (2019) 351–368.
- [47] Y. Liu, K. Ai, L. Lu, Polydopamine and its derivative materials: synthesis and promising applications in energy, environmental, and biomedical fields, *Chem. Rev.* 114 (2014) 5057–5115.